Chapter

Aero Heating Optimization of a Hypersonic Thermochemical Non-Equilibrium Flow around Blunt Body by Application of Opposing Jet and Blunt Spike

Rachid Renane, Rachid Allouche, Oumaima Zmit and Bouchra Bouchama

Abstract

The goal of this work is to give optimum aerothermal solutions for thermal protection of the nose wall of space shuttles during atmospheric reentry, where the air flow is hypersonic, nonequilibrium reactive flow (vibrational and chemical) behind detached shock waves, it's governed by Navier–Stokes equations with chemical reaction source terms, and modelled using five species (N_2, O_2, NO, N, O) and Zeldovich chemical scheme with five reactions. This study which simulates the flow using the software Fluent v.19 focuses on the comparison between three protection techniques based on the repulsion of the shock wave, the first is geometric, it consists in introducing a spike that makes the right shock move away from the nose of the shuttle, this allows the endothermic physicochemical processes of dissociation and ionization to absorb heat, the second technique is based on an opposite jet configuration in the frontal region of the nose, this jet allows to push the strong shock, and consequently reduce the heat released, the last technique is the assembly of the two previous techniques; Jets nearby the spike noses were set up in front of the blunt body to reconfigure the flow field and reduce aerodynamic overheating. The opposing jet model reduces the heat at the nose by 12.08% compared to the spike model and by 20.36% compared to the spike jet model. The flow field reconfiguration was the most important factor in heat reduction, according to the quantitative analysis, a combination parameter was given as the main criterion for designing spiked bodies with opposing jets for the goal of heat reduction based on the locations of the reattached shock and its interaction with the conical shock. The results obtained are in good agreement with the specialized literature.

Keywords: hypersonic reactive flows, non-equilibrium, dissociation, opposing jet, blunt spike, Lobb sphere

1. Introduction

The concept of hypersonic flight has attracted worldwide attention since it was proposed in the 1940s [1–3]. Since there, different hypersonic vehicles were developed as well as hypersonic missiles, aircraft and re-entry vehicles. However, the significant number of technical challenges have surfaced which are critical to the successful development of these high-speed flight vehicles. Understanding, analyzing and predicting high-speed flow around blunt bodies pose a practical and important engineering problem; faster and better design of new flight vehicles depends on it. The high heat of a hypersonic aircraft during flight imposes severe demands on the materials and structures, so the reduction of heat transfer rate plays an important role during the conceptual design of re-entry vehicles. Classical thermal protection systems such as ablatives [4] are less adapted to the rapid growth of spacecraft technology: ablatives are related to the coating thickness, and are not convenient for shape change. To improve the flow field in front of a vehicle nose, additional solutions such as active cooling approach aero-spikes [5] and opposing jets [6] have been developed. Different strategies exhibit varying characteristics in a hypersonic flow field.

The concept of a spiked blunt body was first proposed by Bogdonoff [7]. Flow separation in front of blunt bodies at supersonic speeds, have been made since the early 1950s [8–11]. Spikes have been shown to create a separation zone over blunt bodies, lowering the aerodynamic heat rate and pressure distribution, which is beneficial for thermal protection and drag reduction. In the 1960s, separation characteristics and the resulting flow instability have been the subject of extensive research. Maull explored the effects of spike length and shape on the flow field properties of blunt bodies, concluding that flow oscillation was generated by two factors: shock wave-induced separation and flow reattachment [12]. Using a mix of spike lengths and cone angles, wood explored spiked cone cylinders flying at Mach 10 and established five possible flow patterns with related scopes [13]. Reding et al. examined unstable aerodynamics for a spiky drag reduction device based on structure deflection coupled with thermal expansion generated by aerodynamic heating. Many studies on numerical simulations and solutions have allowed for a great level of insight with regards to spiked blunt bodies since the rapid rise of computer technology began in the 1990s. Many of these researches were validated by collaboration between experiments and numerical simulations. Mehta investigated the relationship between the aerodynamic heat flux and pressure distribution over spiked bodies at Mach 6.8 [14].

The opposing jet technique was introduced initially by Lophtoff [15] and Warren [16], and its obvious effects on drag and heat reduction for aircraft were realized. The interaction between the opposing jet and the free stream determines the flow pattern. Hayashi et al. [17, 18] investigated the opposing jet using both experimental and numerical methods in several investigations. Their tests were carried out in a traditional blow-down type wind tunnel with a free stream of Mach 3.98, and the axisymmetric Navier-Stokes equations were solved using the implicit finite difference method. Their research revealed that the ratio of the opposing jet's stagnation pressure to that of the free stream had a significant impact on the flow mode. Isao Tamada et al. [19] investigated the heating reduction of the ogive body and hemispherical nose cylinder body experimentally and numerically, at M = 3.98 and M = 8.0. They found that local Reynolds number management and recompressed shock monument are critical to reducing aerodynamic heating, and that the ogive body was more effective at reducing heating with the same mass flow rate because of its large enough recirculation region to cover the entire nose tip.

Huang et al. [20, 21] investigated some opposing jet configurations with other cooling approaches, such as spike, aerodisk, and forward-facing cavity, and discovered combined promising drag and heat flux reduction effects, as well as the coupling mechanism between the self-sustained oscillations induced by the jet and the unsteady modes induced by the other configurations. An experiment was conducted by Jiang et al. [22] which a new concept of the non-ablative thermal protection system for hypersonic vehicles was first proposed, and the blunt spike was combined with lateral jets for developing a shock reconstruction system at the front side of hypersonic vehicles, to achieve effective wave for reducing drag under non-zero attack angles and also to avoid severe aero heating (rocket).

In this work, a blunt re-entry vehicle is modeled and analyzed in ANSYS Fluent 19 which represents the distribution of heat flux on the surface of a representative Lobb sphere blunt body and the coupled effects of thermochemical non-equilibrium and chemical reactions on the hypersonic air flows. Validation is performed with the obtained CFD results which are in good agreement with the experimental values of Liu and Jiang [23] for blunt spike body and Hayashi et al. [24] for opposing jet. Next, optimization is carried out by placing a jet at the front of the blunt spike body. The main simulation results are discussed by comparing the spike and jet heat reduction configurations.

2. Mathematical and physical modeling

The two-dimensional, steady, compressible, Navier Stokes equation set was applied as the governing equations. The fundamental governing equations are represented in Eqs. (1)–(6). The density was calculated using the ideal gas law. For viscous and compressible flow, the viscosity is generally [25] calculated as a function of temperature as defined by Armally and Sutton law as in Eq. (7), and hence it is used in the present work.

2.1 Species conservation

For species in a mixture, the mass conservation equation is dictated by:

$$\underbrace{\frac{\partial \rho_\alpha}{\partial t}}_{1} + \underbrace{\frac{\partial}{\partial x}\left(\rho_\alpha u - \left(-q^D_{\alpha x}\right)\right)}_{2} + \underbrace{\frac{\partial}{\partial y}\left(\rho_\alpha u - \left(-q^D_{\alpha y}\right)\right)}_{3} = \underbrace{\dot{w}_\alpha}_{4} \tag{1}$$

The global continuity equation is given by

$$\underbrace{\frac{\partial \rho}{\partial t}}_{1} + \underbrace{\frac{\partial}{\partial x}(\rho u)}_{2} + \underbrace{\frac{\partial}{\partial y}(\rho u)}_{3} = 0 \tag{2}$$

2.2 Global momentum conservation

The mixture's momentum balance is given by

$$\underbrace{\frac{\partial \rho u}{\partial t}}_{1} + \underbrace{\frac{\partial}{\partial x}\left(\rho u^2 + p - \tau_{xx}\right)}_{2} + \underbrace{\frac{\partial}{\partial y}\left(\rho uv - \tau_{xy}\right)}_{3} = 0 \tag{3}$$

$$\underbrace{\frac{\partial \rho v}{\partial t}}_{1} + \underbrace{\frac{\partial}{\partial x}\left(\rho uv - \tau_{xy}\right)}_{2} + \underbrace{\frac{\partial}{\partial y}\left(\rho v^2 + p - \tau_{yy}\right)}_{3} = 0 \tag{4}$$

2.3 Vibrational energy conservation

Vibrational energy conservation is a phenomenological characterization of the average energy in each molecular species' vibrational mode. The conservation of vibrational energy is regulated by:

$$\underbrace{\frac{\partial}{\partial t}\left(\rho_m e_m^{vib}\right)}_{1} + \underbrace{\frac{\partial}{\partial x}\left(\rho_m e_m^{vib} u - q_{mx}^{vib}\right)}_{2} + \underbrace{\frac{\partial}{\partial y}\left(\rho_m e_m^{vib} v - q_{my}^{vib}\right)}_{3} = \underbrace{\Omega_m}_{4} \tag{5}$$

2.4 Total energy conservation

Total energy conservation (internal + kinetic) is regulated by

$$\underbrace{\frac{\partial(\rho E)}{\partial t}}_{1} + \underbrace{\frac{\partial}{\partial x}(\rho E + p)u - \left(u\tau_{xx} + v\tau_{\gamma x} + qt_x\right)}_{2} + \underbrace{\frac{\partial}{\partial y}\left((\rho E + p)v - \left(u\tau_{xx} + v\tau_{\gamma x} + q_\gamma t\right)\right)}_{3} \tag{6}$$

2.5 Armaly Sutton law

$$\mu_\alpha = 0.1\ exp\left[\left(A_\alpha^\mu ln\,(T) + B_\alpha^\mu\right) ln\,(T) + C_\alpha^\mu\right] \tag{7}$$

2.6 Chemical kinetic model

A thermo-chemically non-equilibrium flow of a five-component air model consisting of species N_2, O_2, NO, N and O was considered. We have made the hypothesis of a chemical flow at vibrational equilibrium; the ionization phenomena have been neglected. The most important chemical reactions between these species are: [26, 27].

$$N_2 + M \rightleftharpoons 2\,N + M \tag{8}$$

$$O_2 + M \rightleftharpoons 2O + M \tag{9}$$

$$NO + M \rightleftharpoons N + O + M \tag{10}$$

$$NO + O \rightleftharpoons N + O_2 \tag{11}$$

$$N_2 + O \rightleftharpoons NO + N \tag{12}$$

The chemical source names are formed from reactions that take place between the gas's constituents. A mass transfer mechanism occurs between species as reactions occur so the formulas for these mass transfer rates are determined. Several separate elementary chemical reactions between species in the gas can take place at the same time. Consider the r^{th} chemical reaction of N_r elementary reactions between N_s chemically reacting species:

$$\sum v'_{\alpha,r} X_\alpha = \sum v''_{\alpha,r} X_\alpha \tag{13}$$

There is a forward and backward portion to the chemical reaction equation, Eq. (13). The forward and backward reaction rates are calculated as follows:

Forward:

$$\frac{d[X_\alpha]_r^f}{dt} = \left(v''_{\alpha,r} - v'_{\alpha,r}\right)\left[k_{f,r}\prod_{\alpha=1}^{N_s}[X_\alpha]^{v'_{\alpha,r}}\right] \tag{14}$$

Backward:

$$\frac{d[X_\alpha]_r^b}{dt} = \left(v''_{\alpha,r} - v'_{\alpha,r}\right)\left[k_{b,r}\prod_{\alpha=1}^{N_s}[X_\alpha]^{v''_{\alpha,r}}\right] \tag{15}$$

Where

- $k_{f,\,r}$ and $k_{b,\,r}$ are the forward and backward reaction rate coefficients of reaction r, which are both affected by the temperature of the reaction.

The net rate for the above general reaction r can be written as

$$\frac{d[X_\alpha]}{dt} = \frac{d[X_\alpha]_r^f}{dt} - \frac{d[X_\alpha]_r^b}{dt} = \left(v''_{\alpha,r} - v'_{\alpha,r}\right)\left[k_{f,r}\prod_{\alpha=1}^{N_s}[X_\alpha]^{v'_{\alpha,r}} - k_{b,r}\prod_{\alpha=1}^{N_s}[X_\alpha]^{v''_{\alpha,r}}\right] \tag{16}$$

The equation above is a general form of the law of mass action, which assures that total mass is preserved during a chemical reaction.

The FLUENT uses the expression given by the law of ARRHENIUS to calculate the direct speed constant. The expression of ARRHENIUS is given by:

$$K_{f,r} = C_{f,r}T_{f,r}^{n_{f,r}}e^{\frac{-E_{f,r}}{kT_{f,r}}} \tag{17}$$

3. Numerical modeling

For aerodynamic flow, Reynolds-Average Navier-Stokes (RANS) equations are adopted as the governing equations. The convective terms are approximated by the AUSM-DV scheme [28] with a MUSCL approach to increase the numerical accuracy. The turbulence model is required for several shear layers including the boundary layer, The k-ω model (SST) [29] model in the region close to the wall was used.

3.1 Computational model

The structures of a Lobb sphere blunt body are shown in **Figure 1**. The diameter of the body is 6.35 mm with a length of 1.3 mm [30]. The geometry in **Figure 1** was created in a way that the simulation will be run using the axisymmetric Navier-Stock's equations, therefore, a two-dimensional symmetric geometry is created, with an axis defined at the radial centre of the studied body. This technique makes it possible to reduce the computational domain used and consequently reduce the calculation time.

Then we set up an opposing jet in the same Lobb sphere with a radius of 0.5 mm as shown in **Figure 2**.

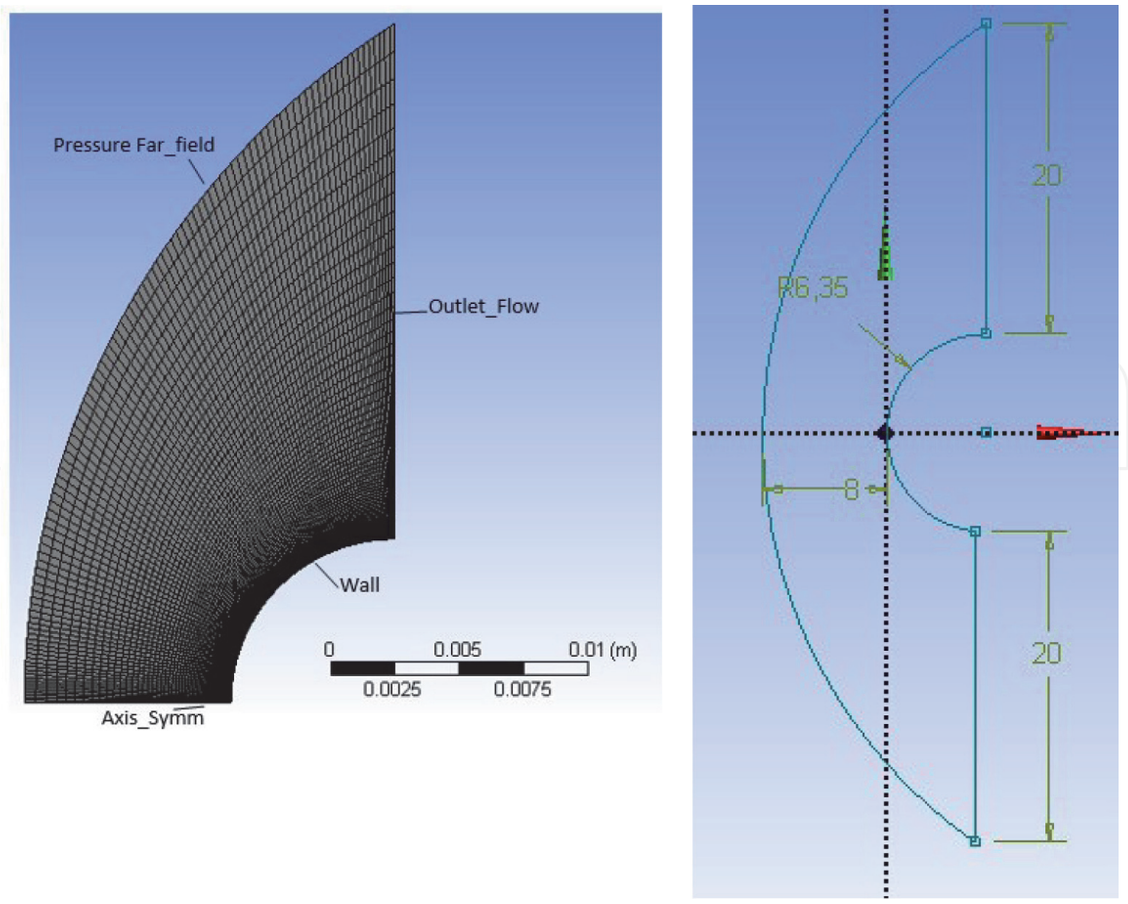

Figure 1.
Lobb sphere mesh and geometry.

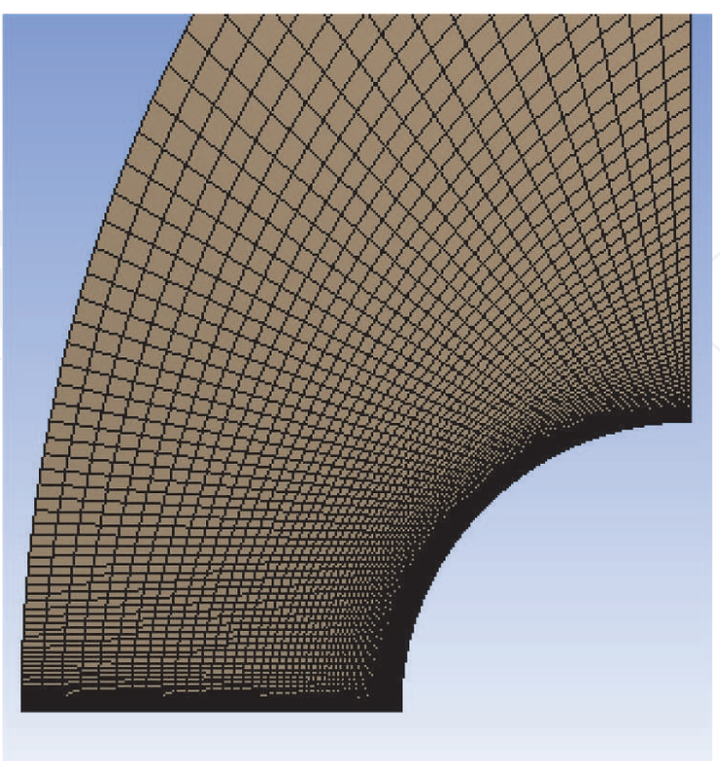

Figure 2.
Lobb sphere with opposing jet mesh and geometry.

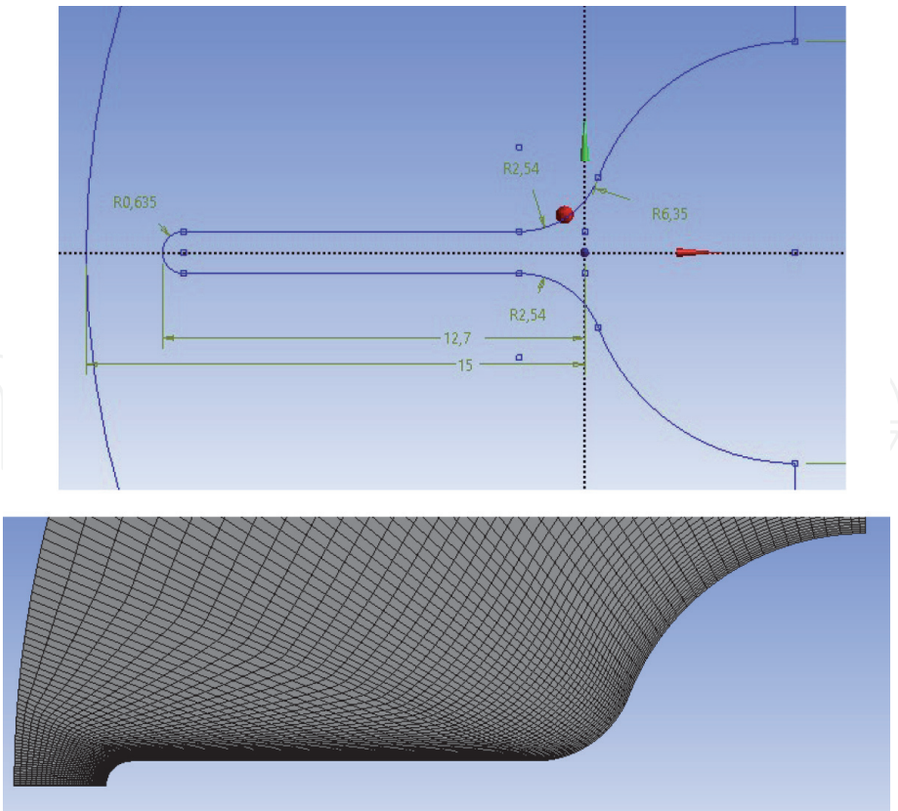

Figure 3.
Blunt spike mesh and geometry.

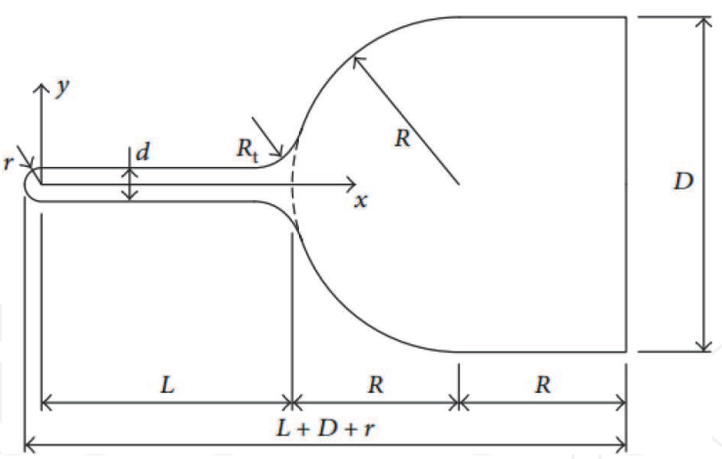

Figure 4.
Configuration of the spiked blunt body for simulation [31].

Next, we install the second heat reduction configuration, the blunt Spike in front of the same Lobb sphere body profile to reconfigure the flow field and reduce the overheating in a re-entry hypersonic flight as shown in **Figure 3**. **Figure 4** shows the configuration and dimensions of the spiked (4) [31].

- The characteristic dimensional are d/D = 0.1, L/D = 0.9 and Rt/D = 0.2 where:

  D: is the diameter of the spherical head profile, d: is the diameter of the spike,

  L: is the spike length and Rt: is the transition part radius at the spike root.

3.2 Mesh independence

An appropriate grid appears to be the key to numerical prediction accuracy, particularly in the case of aerodynamic heating prediction. A grid independence investigation was undertaken over multiple grid densities before initiating the CFD simulations. Because the heat transfer between the surrounding air and the vehicle wall was so important in this research, attention has been devoted to the near-wall mesh quality.

In the Lobb sphere blunt body, five-level grids are employed, and the details of these grids are shown in **Table 1**. The region located near the wall has meshed with a gradient structured mesh. The flow temperature for different grids is shown in **Figure 5**, we notice that the more the grid is refined more the temperature is stable where the result starts to be independent of the mesh. As computational time depends on the size of the grid. Thus the grid of case 4 is used in the following simulations with considering the calculation efficiency.

Adaption	Initial	Adaption1	Adaption2	Adaption3	Adaption4	Adaption5
Cells	2500	4858	10,570	25,146	80,974	129,963
Nodes	5601	7054	15,990	11,575	37,546	89,125
T(K)	8743.415	9193.686	9691.146	9808.36	10,130	10,280

Table 1.
Lobb sphere grid independency.

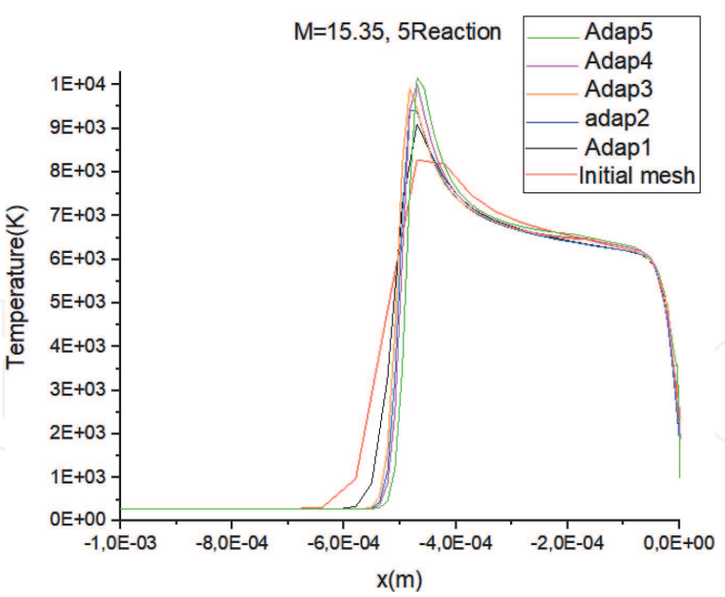

Figure 5.
Lobb sphere grid independency.

Adaption	Initial	Adaption1	Adaption2	Adaption3
Cells	5000	14,330	52,787	53,360
Nodes	14,626	14,626	53,376	53,948

Table 2.
Blunt spike configuration grid independency.

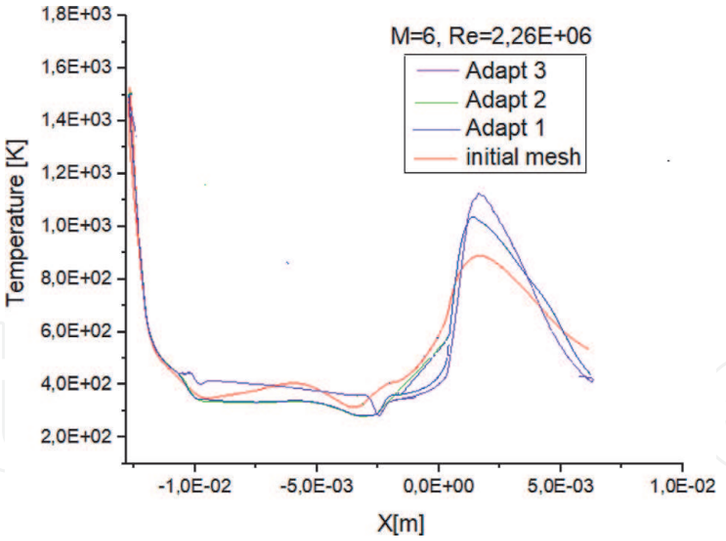

Figure 6.
Blunt spike grid independency.

Always by the same refinement method, the sensitivity test for the spike mesh was performed for three different mesh densities (**Table 2**). We notice that the result become independent of mesh from adapt 2 because the variation of temperature is no longer observed during the refinement in **Figure 6**, from adapt 2 with a temperature of 11123 k to adapt 3 with temperature 11232 k so we can consider that the "adapted 2 mesh" is the optimum mesh.

4. Validation of numerical models

4.1 Validation of Lobb sphere blunt body

By comparing our result of **Figure 7** with that of Tristan [30] which shows the variation of the temperature along with the relaxation range, one notices a good agreement between the two results in terms of pace and the quantitative terms. The slight difference is because Tristan considered a flow out of vibrational equilibrium. The study was simulated under the flowing free stream conditions (**Table 3**).

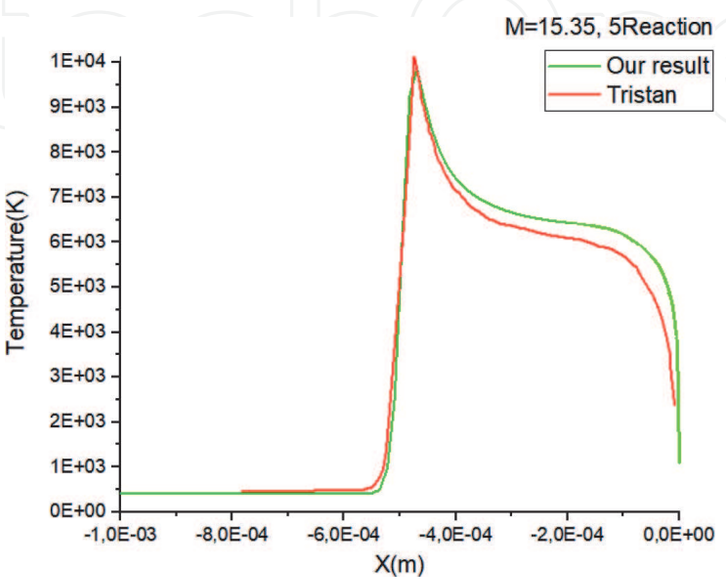

Figure 7.
Temperature along the stagnation ling.

M_∞	Reaction.N	$T_\infty[k]$	$\rho_\infty(\mathrm{kg/m^3})$	P_∞ [Pa]	K	ω
15.35	5	293	$7.896\ 10^{-3}$	664	3245.962	64.607

Table 3.
Lobb sphere free stream boundary condition [30].

Source	Shock position [mm]
Present results	0.536
Tristan	0.535
Tchuen	0.531
Joly et al	0.598
S'eror	0.557
Lobb	0.552 ± 0.032

Table 4.
Position of the shock of the Lobb sphere [30].

Table 4 illustrates that this result agrees well with the experimentally determined value with an error of 2.89% [32] and the numerical values obtained in the literature [33, 34].

4.2 Validation of spike blunt configuration

The numerical solution validation was carried out by comparing the experimental flow field as shown in **Figure 8**. The conditions were set as M_∞ = 6, Re = 2.26E+2 and L/D = 1.0 [31]. Numerical and experimental results are in agreement, indicating the main flow field structures, including conical shock, reattached shock, slip line, shear layer, and separation zone.

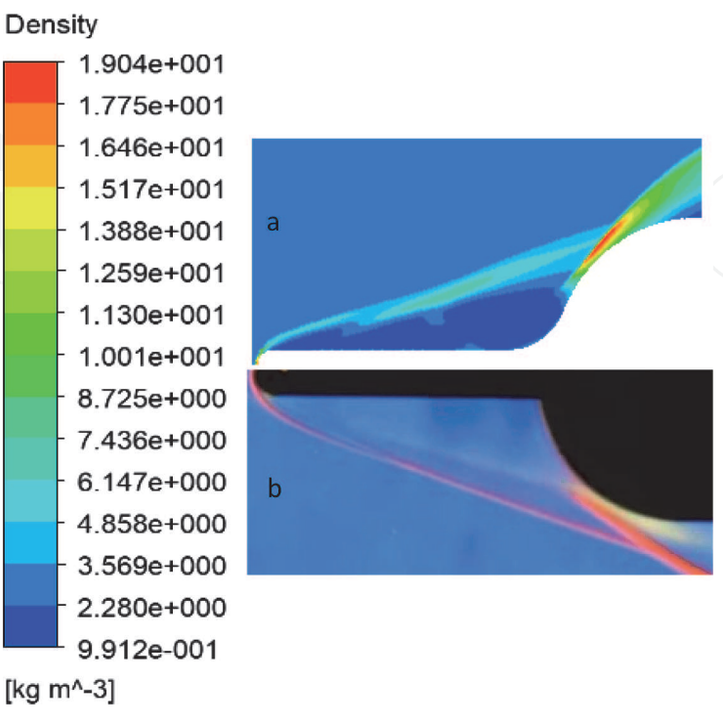

Figure 8.
Flow field wave structure of the spiked blunt body with spike length L/D = 1.0; (a) our numerical photograph result; (b) experimental Schlieren photograph [23].

4.3 Validation of opposing jet configuration

Numerical results are compared with the experiment by NASA Langley in 1987 [24]. The radius of the cylinder is 25.4 mm and the thickness of the steel is 12.7 mm [35] (**Figure 9**). The free flow parameters are as follows (**Table 5**).

To investigate the effect of thermal protection systems we carried out a comparison between the opposing jet model and spike model at 26 km under the following free stream conditions illustrated in **Table 6**.

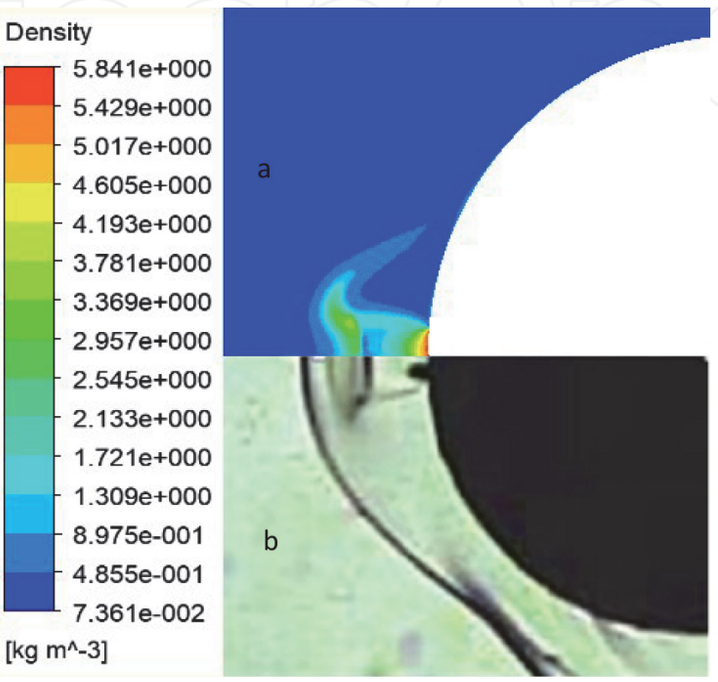

Figure 9.
Flow field wave structure of opposing jet; (a) our numerical photograph result; (b) experimental Hayashi photograph [24].

Free stream	The opposing jet	The wall
Gas: Air Mach number: 3.98 Total pressure: 1.37 MPa Total temperature: 397 K	Gas specified in mole fraction: 0.2571 CO_2, 0.3142 N_2, 0.4287 $H_2O(g)$ Mach number: 1 Total pressure ratio: 0.4 Total temperature: 200 K	Temperature 295 K

Table 5.
Opposing jet free stream boundary condition [35].

Free stream	Opposing jet		Wall condition
• Gas: air • Mach number: 6 • Total pressure: 4.02 MPa • Total temperature: 1812 K	Pressure ratio: 1.25 Total temperature: 300 K	**Sizing** 1. Opossing jet diameter 1 mm 2. Assembly of spike and jet 0.15 mm	Convection with heat transfer coefficient 1577 (W/m^2 K) according to [36, 37]

Table 6.
Boundary condition and sizing.

5. Discussion and results

5.1 Spike effect

We observed that the shock wave scattered along the length and decreases the temperature in the vehicle nose surface from 1254 to a value of 1053 k from spike nose to the body nose respectively as noticed in **Figure 10**. The presence of the spike, blunt transforms the bow shock into a weaker conical shock.

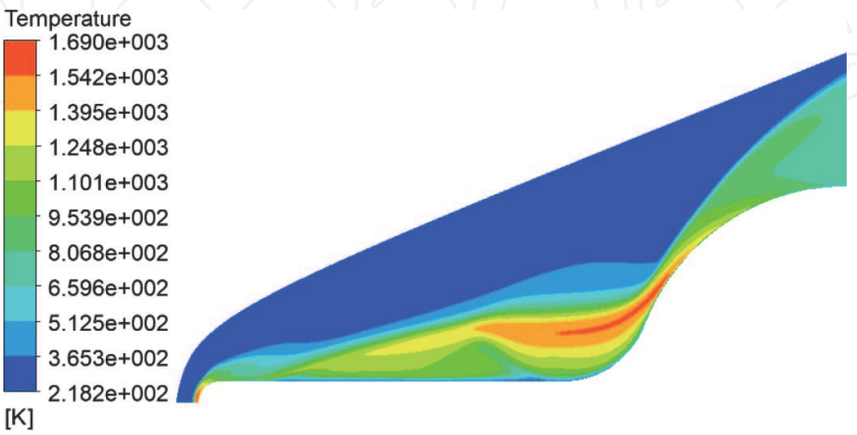

Figure 10.
Blunt spike temperature distribution.

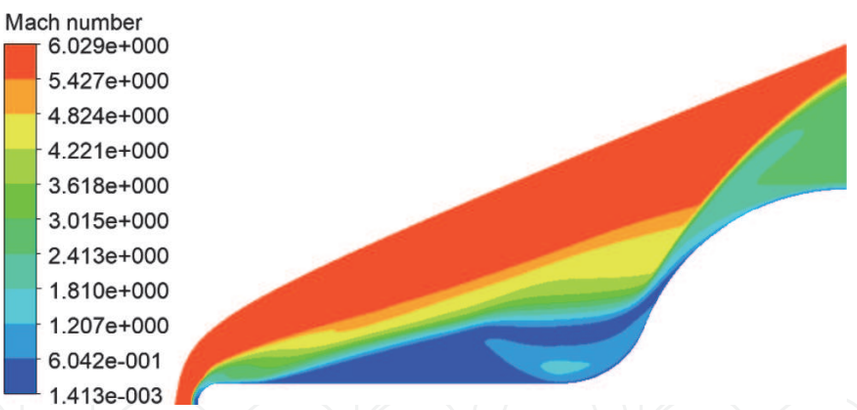

Figure 11.
Blunt spike Mach number distribution.

Figure 12.
Blunt spike pressure distribution.

Figure 13.
Blunt spike density distribution.

The high-speed flow traveled to the blunt body shoulder as shown in **Figure 11**, result in a reattached shock formation with a high-pressure zone in **Figure 12**, the unfavorable pressure gradient inverses the gas flow to the spike nose. Thus, a circumfluence zone was generated around the spick and the blunt body nose which induce a lower velocity than that after the conical shock, generating a shear layer.

represented in **Figure 13**, which reduces some of the fluid in the circumfluence area. So, the combined effect of the reduced foreshock and the recirculation zone on the main body can result in significant reductions in aero heating estimated by 16.67%.

5.2 Jet effect

Figure 14 represent the distribution of pressure, temperature, density and streamlines of the fluid field with opposing jet configuration shows that the jet layer reattaches to the blunt body surface, and then a low temperature recirculation region is formed lead to the formation of a normal shock ward off from the blunt body nose. Where a recompression shock wave also formed downstream the reattachment region of the jet layer.

The interaction between the flow field and the solid structure determines the heating rate distributions. The temperature difference between the solid external surface and the fluid layer near the fluid-solid interface will change as the temperature field of the solid structure changes due to aerodynamic heating, which will affect in turn the heat transfer between the fluid and the solid domain. so, by introducing the opposing jet configuration the temperature was reduced from 1035 without jet to 854 with jet model, this led to a heat flux reduction estimated by 28.75%.

5.3 Comparison between spike and jet configuration

Figure 15 shows that spike configuration ward off the shock wave from the blunt body nose by 0.01 m were the spike nose faces the maximum temperature by reducing the blunt body temperature by 16.67% from the blunt nose body, this configuration, by its virtue of geometry and nose sizing which are smaller compared to blunt body nose, admit the use of refractory material that can withstands very high temperatures such as zirconium only on the nose of the spike instead of all the blunt body nose, this will reduce the economic cost of the spacecraft design. Compared with jet cooling configuration, the direct interaction between the jet gaze's

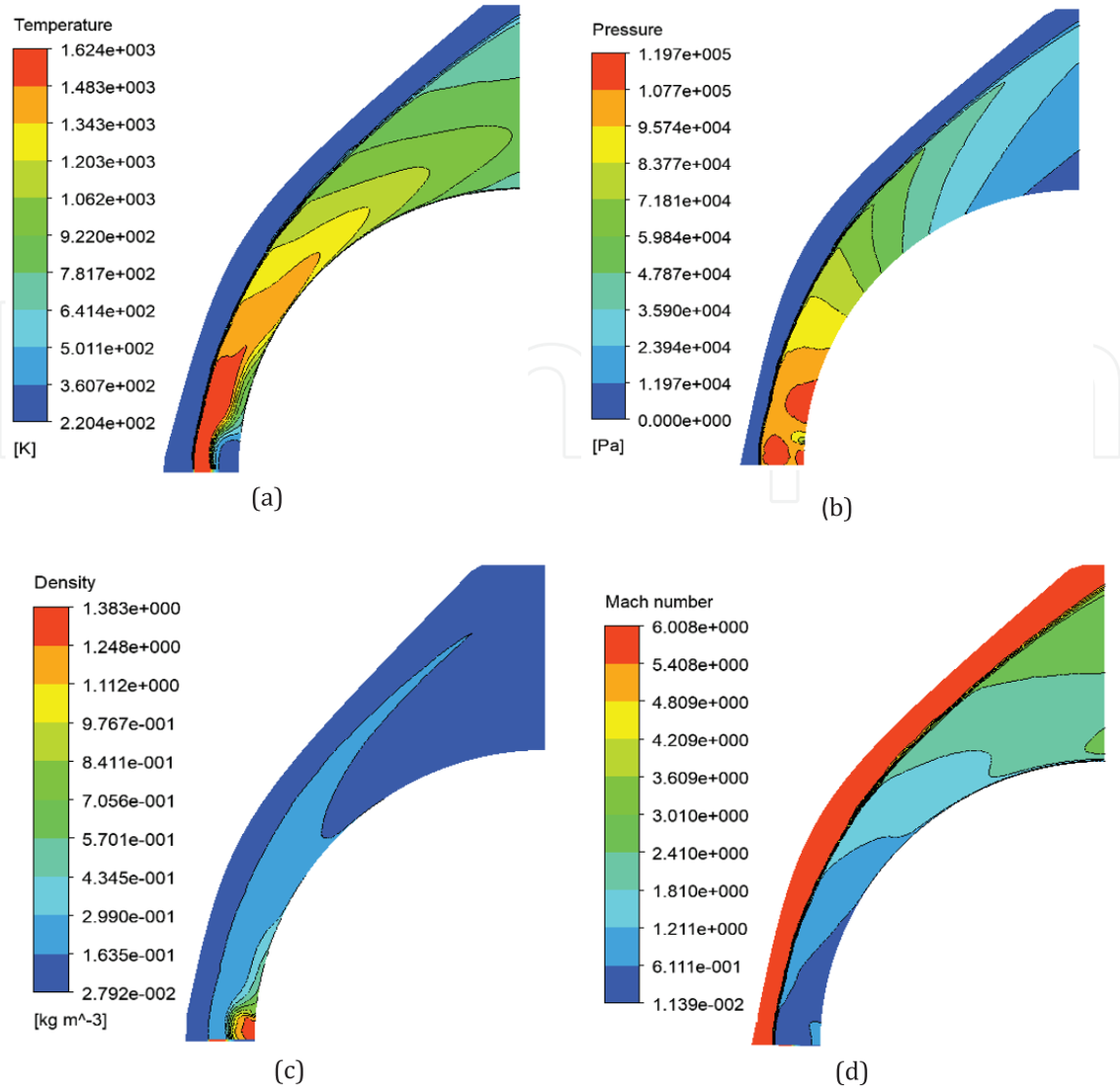

Figure 14.
Jet configuration properties. (a) Opposing jet temperature distribution; (b) opposing jet pressure distribution; (c) opposing jet density distribution; (d) opposing jet Mach number distribution.

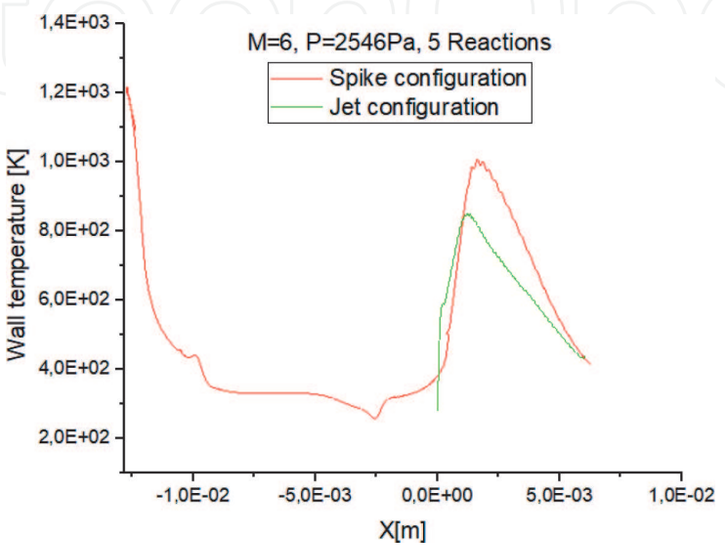

Figure 15.
Opposing jet and bunt spike wall temperature distribution.

and free stream flow, induces a redistribution of the temperature in the mixing zone ward off the normal shock from the nose blunt body about 0.3 mm, which allows the reduction of the wall heat transfer of the body by approximately 28.75%, this cooling system must be associated with important subsystems, particularly in terms of feasibility constrained by the mass and layout problems (regulator, pump, storage tank of gaze, etc.).

5.4 Jet spike configuration

To reduce the huge heat load in the small area of the spike nose, we have proposed an assembly between the spike and the opposing jet configuration by introducing a jet into the nose of the spike to protect the nose from the overheating temperatures and minimize the cost of conventional thermal protection systems such as zirconium. **Figure 16** depicts the velocity of the velocity distribution in the analysis models with and without an opposing jet. The spike generates flow separation in the analytical model without an opposing jet, forming a primary recirculation zone in front of the blunt body. The major recirculation zone in the analytical model with opposing jet is substantially larger than in the model without opposing jet. The reason for this is because the recirculation zones generated by the spike and opposing jet squeeze and interfere with one another, resulting in the formation of a third recirculation zone in the middle. A larger main recirculation zone is formed by these three recirculation zones. This configuration limits the overheat load concentrated just in the frontal nose of the spike as shown **Figure 17**, this limits the cost of the thermal protection system needed in the nose area in the case without jet.

Figure 18 represent the wall temperature for the two configurations spike and the assembly of the two systems, we notice that opposing jet spike have a better effect on the heat flux reduction with 502 K wall temperature compared to the spike configuration with 1205 K in the spike nose area by a reduction estimated by 58.33%.

Instead, the huge reduction in wall temperature is due to the initial jet temperature set of 300 K, where thermal equilibrium occurs between the flow near the wall and the initial jet flow [24].

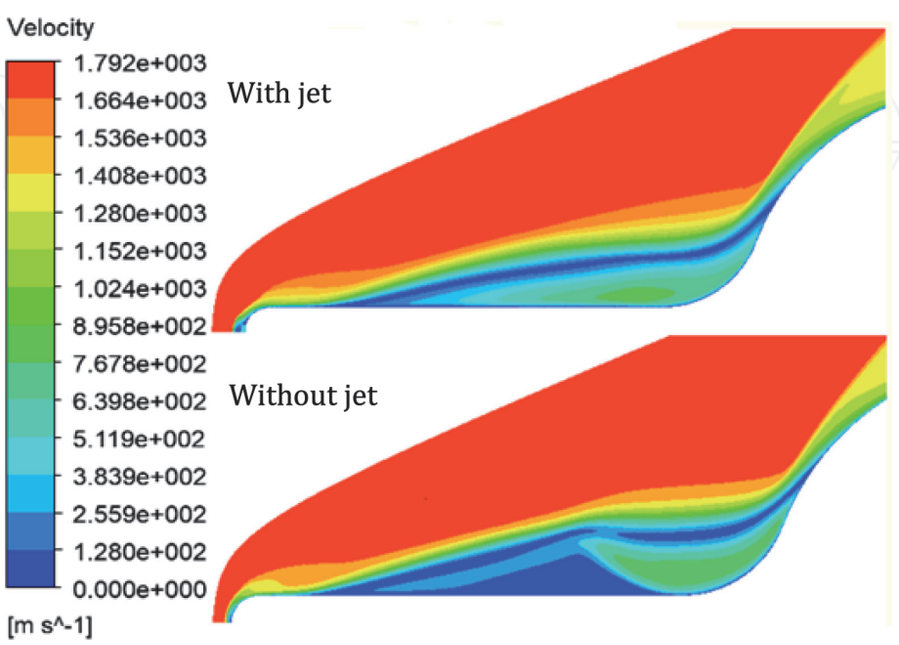

Figure 16.
Velocity distribution of analysis models with and without opposing jet.

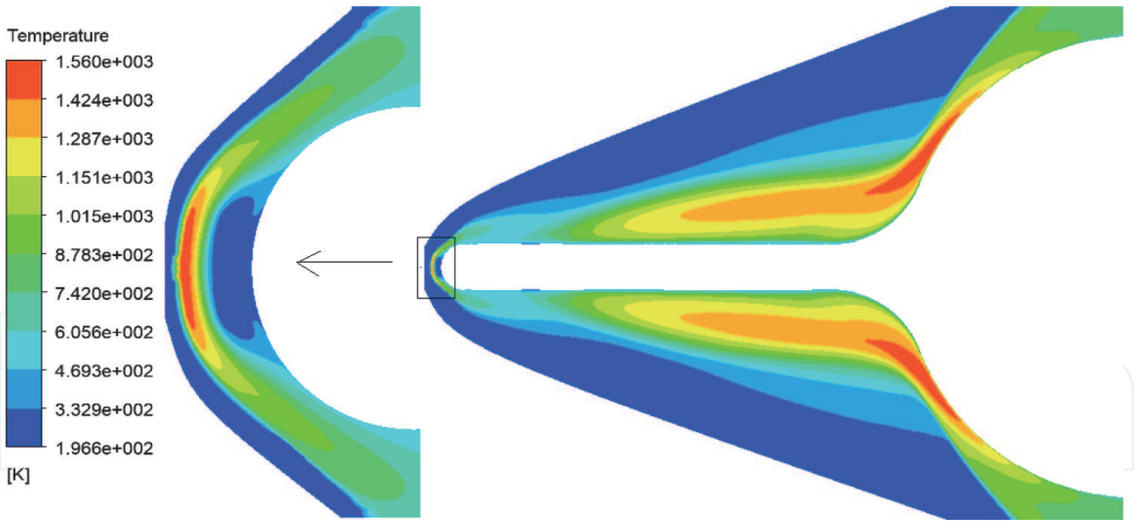

Figure 17.
Jet spike configurations.

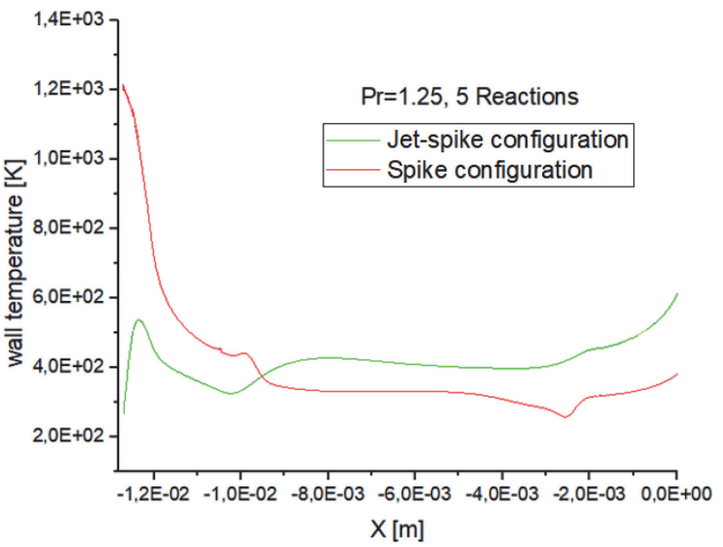

Figure 18.
Wall temperature along with deferent configurations.

6. Conclusion

This study numerically investigates three thermal protection systems that have good potential to reduce the critical heat flux imparted to the blunt-bodies vehicle during its atmospheric reentry, the efficiency of opposing jet, and spike configuration have been discussed and the major conclusions established in this study are summarized as follows:

- The opposing jet configuration isolates the body from the wall from the large hypersonic heat flux, which minimizes the temperature of the stagnation zone in the blunt body of the nose by minimizing the thermal transfer between the flux and the wall by approximately 28.75%, creating an area of recirculation that moves the shock wave slightly away from the tip of the nose; as a result, reducing the heat fluxes transferred to the reentry vehicle walls using opposing jet has a significant interest in the aerospace industry that raises important questions, particularly about the feasibility caused by problems of mass and arrangement layout problem.

- The presence of a spike in a hypersonic flow generates conical shocks in front of the blunt body, a reattached shock settles in the shoulders, and the flow behind the conical shock reattaches to the radial limits of the blunt body, and under the influence of the pressure gradient, it forms a reattached shock. For stable aerodynamic and thermochemical conditions, a phenomenal and endothermic equilibrium is established between the conical shock, the reattached shock and the blunt body, which cause an estimated heat reduction of 16.67% presented in **Figure 15**.

- The jet-spike configuration reduces the heat flux in the spike nose region from 1205 K to 502 K with and without opposing jet respectively, by a reduction estimated by 58.33%.

- In quantitative terms and according to **Figures 15** and **18**, the opposite-jet configuration technique is the best configuration which reduces the near-wall temperature more by 12.08% compared to the spike-configuration, but it remains (spike-configuration) the most practical technique.

Conflict of interest

None declare.

Nomenclature

α	chemical species
E	total specific energy (j/kg)
$E_{f,r}$	activation energy for reaction r (J/kg)
e	specific internal energy (J/kg)
$K_{f,r}$	forward reaction rate coefficient in S.I.
$K_{f,b}$	backward reaction rate coefficient in S.I.
N_r	total number of reactions
N_s	total number of species
m	diatomic species
P	pressure (N/m^2)
q	heat flux (J/m^2 s)
q_α^D	mass diffusion flux of species α ($kg/(m^2$ s))
S	entropy (J/K)
t	time (s)
$T_{f,r}$	temperature of forward reaction r (K)
u, v	speed in x and y directions (m/s)

Author details

Rachid Renane*, Rachid Allouche, Oumaima Zmit and Bouchra Bouchama
Laboratory of Aeronautical Sciences, Institute of Aeronautics and Space Studies, University of Blida1, Algeria

*Address all correspondence to: r.renane@gmail.com

IntechOpen

References

[1] Allouche R, Renane R, Haoui R. Prediction of the optimal speed of an aerospace vehicle by aerothermochemical analysis of hypersonic flow during atmospheric re-entry. Mechanics & Industry. 2020;**21**:208

[2] Allouche R, Haoui R, Renane R. Numerical simulation of reactive flow in non-equilibrium behind a strong shock wave during re-entry into earth's atmosphere. Mechanics & Industry. 2014;**15**:81-87

[3] Anderson JD Jr. Hypersonic and High-Temperature Gas Dynamics. 2nd ed. USA: AIAA Education Series; 2006

[4] Venkatapathy E, Laub B, Hartman GJ, Arnold JO, Wright MJ, Allen GA Jr. Thermal protection system development, testing, and qualification for atmospheric probes and sample return missions: Examples for saturn, titan and stardust-type sample return. Advances in Space Research. 2009; **44**(1):138-150. DOI: 10.1016/j.asr.2008.12.023

[5] Barzegar Gerdroodbary M, Hosseinalipour SM. Numerical simulation of hypersonic flow over highly blunted cones with spike. Acta Astronautica. 2010;**67**:180-193. DOI: 10.1016/j.actaastro.2010.01.026

[6] Barzegar Gerdroodbary M et al. Transient analysis of counterflowing jet over highly blunt cone in hypersonic flow. Acta Astronautica. 2012;**73**:38-48. DOI: 10.1016/j.actaastro.2011.12.011

[7] Bogdonoff SM. Preliminary investigations of spiked bodies at hypersonic speeds. Journal of the Aerospace Sciences. 1959;**26**(2):65-74

[8] Moeckel WE. Flow separation ahead of blunt axially symmetric body at Mach number 1.76 to 2.10. NACA RM, article E51I25. 1951

[9] Moeckel WE. Flow separation ahead of blunt bodies at supersonic speeds. NACA TN. Vol. 2418. 1951

[10] Stadler JR, Nielsen HV. Heat transfer from a hemisphere-cylinder equipped with flow-separation spikes. NACA TN. Vol. 3287. 1954

[11] Kennedy EC. Calculation of axisymmetric isentropic spike surfaces. Journal of the Aerospace Sciences. 1958; **25**(7):463-464

[12] Maull DJ. Hypersonic flow over axially symmetric spiked bodies. Journal of Fluid Mechanics. 1960;**8**(4):584-592

[13] Wood CJ. Hypersonic flow over spiked cones. Journal of Fluid Mechanics. 1962;**12**(4):614-624

[14] Mehta RC. Numerical heat transfer study over spiked blunt bodies at Mach 6.8. Journal of Spacecraft and Rockets. 2000;**37**(5):700-703

[15] Lopatoff M. Wing-flow study of pressure drag reduction at transonic speed by projecting a jet air from the nose of aprolate spheroid of fineness ratio of 6. Journal of Spacecraft and Rockets. NACA RL51E09. 1951. DOI: 10.1017/S0022112060000694

[16] Warren CHE. An experimental investigation of the effect of ejecting a coolant gas at the nose of a bluff body. Fluid Mechanics. 1960;**8**:400-417. DOI: 10.1017/S0022112060000694

[17] Hayashi K, Aso S, Tani Y. Numerical study of thermal protection system by opposing jet. In: 43rd, AIAA Aerospace Sciences Meeting and Exhibit, AIAA 2005-188. NV: Reno; 2005

[18] Hayashi K, Aso S, Tani Y. Experimental study on thermal protection system by opposing jet in supersonic flow. Spacecraft Rockets.

2006;**43**(1):233-235. DOI: 10.2514/1.15332

[19] Isao T, Shigeru A, Yasuhiro T. Reducing Aerodynamic Heating by the Opposing Jet in Supersonic and Hypersonic Flows, AIAA 2010-991. Florida; 2010

[20] Huang W. A survey of drag and heat reduction in supersonic flows by a counterflowing jet and its combinations. Journal of Zhejiang University Science A. 2015;**16**(7):551-561. Available from: https://link.springer.com/content/pdf/10.1631/jzus.A1500021.pdf

[21] Huang W, Chen Z, Yan L, Yan B, Du Z. Drag and heat flux reduction mechanism induced by the spike and its combinations in supersonic flows: a review. Progress in Aerospace Science. 2019;**105**:31-39. DOI: 10.1016/j.paerosci.2018.12.001

[22] Jiang Z, Liu Y, Han G. A new concept of the non-ablative thermal protection System (NATPS) for hypersonic vehicles. 2013;**51**(3): 584-590

[23] Liu Y, Jiang Z. Concept of non-ablative thermal protection system for hypersonic vehicles. AIAA Journal. 2013;**51**(3):584-590

[24] Hayashi K, Aso S, Tani Y. Experimental study on thermal protection system by opposing jet in super-sonic flow. Journal of Spacecraft and Rockets. 2006;**43**(1):233-235. DOI: doi.org/10.2514/1.15332

[25] Armaly B, Sutton K. Viscosity of multicomponent partially ionized gas mixtures. In: 15th Thermophysics Conference. 1980. p. 1495

[26] Dunn MG, Kang S-W. Theoretical and Experimental Studies Reentry Plasmas. Buffalo, N.Y. 14221 Jor Langley Research Center, National Aeronautics and Space Administration° Washington, D.C.: Cornell Aeronautical Laboratory, INC.; 1973

[27] Ma Y, Zhong X. Numerical simulation of transient hypersonic flow with real gas effects. In: 37th Aerospace Sciences Meeting & Exhibit; January 1; University of California, Los Angeles Los Angeles, CA. NV: Reno; 1999. pp. 1-14

[28] Azevedo JLF, Heidi K. 1998 AIAA 1998-2629

[29] Menter FR. Two-equation eddy-viscosity turbulence models for engineering applications. AIAA Journal. 1994;**32**(8):1598-1605

[30] Soubrie T. Prise en compte de l'ionisation et du rayonnement dans la modélisation des écoulements de rentrée terrestre et martienne. 1er ed. Paris: L'école National Supérieure de L'Aéronautique et de l'espace; 2006

[31] Han G, Jiang Z. Hypersonic Flow Field Reconfiguration and Drag Reduction of Blunt Body with Spikes and Sideward Jets. 4th ed. Beijing, China: State Key Laboratory of High Temperature Gas Dynamics, Institute of Mechanics, Chinese Academy of Sciences; 2017. DOI: 10.1155/2018/7432961

[32] Kennethlobb R. Experimental measurement of shock detachment distance on sphere fired in air at hypervelocity's. In: Nelson WC, editor. Proc. of the AGARD-NATO in The High Temperature Aspect of Hypersonic Flow. 133rd ed. Maryland: Pergamum Press; 1962

[33] Joly V, Coquel F, Marmignon C, Aretz W, Metz S, Wilhelmi H. Numerical Modelling of Heat Transfer and Relaxation in Nonequilibrium Air at Hypersonic Speeds. La Recherche Aerospatiale: Aachen University; 1994

[34] Tchuen G. Modélisation et simulation numérique des écoulements

a haute enthalpie: Influence du déséquilibre électronique. See also AIAA paper 2004–2462 [PhD thesis]. Université d'Aix-Marseille I; 2003

[35] Shen BX, Liu WQ, Yin L. Drag and Heat Reduction Efficiency Research on Opposing Jet in Supersonic Flows. Changsha 410073, China: Science and Technology on Scramjet Laboratory, National University of Defense Technology; 2018

[36] Lester L. Laminar heat transfer over blunt-nosed bodies at hypersonic flight speeds. Jet Propulsion Journal. 1956;**26**: 259-269. DOI: 10.2514/8.6977

[37] Allen HJ, Eggers AJ. A study of the motion and aerodynamic heating of ballistic missiles entering the earth's atmosphere at high supersonic speeds. NACA TR 1381. 1958